Natural $(Mg,Fe)SiO_3$-Ilmenite and -Perovskite in the Tenham Meteorite

Naotaka Tomioka* and Kiyoshi Fujino

The minerals $(Mg,Fe)SiO_3$-ilmenite and -perovskite were identified in the shock-induced veins in the Tenham chondritic meteorite. Both phases are inferred to have transformed from pyroxene at high pressures and temperatures by shock metamorphism. Columnar-shaped ilmenite grains, one of two types of morphologies, have a topotaxial relationship with neighboring pyroxene grains, indicating shear transformation. Granular-shaped perovskite grains showed a diffraction pattern consistent with orthorhombic perovskite, but these grains were not stable under the electron beam irradiation and became amorphous. The higher iron concentration in both phases compared with those experimentally reported may suggest their metastable transition from enstatite because of shock compression.

Pyroxene with $(Mg,Fe)SiO_3$ composition, one of the major minerals of Earth's crust and upper mantle, is known to transform into modified spinel(β) + stishovite, spinel(γ) + stishovite, garnet (at high temperature) or ilmenite (at low temperature), and perovskite structures in order of increasing pressure (*1–5*). Most of these high-pressure phases are considered to be the main constituent minerals of the mantle transition zone and lower mantle. Among these high-pressure polymorphs of $(Mg,Fe)SiO_3$ pyroxene, however, only garnet has been found to occur naturally as majorite garnet (*6–10*). We report the natural occurrence of $(Mg,Fe)SiO_3$-ilmenite and -perovskite in the Tenham chondritic meteorite.

The Tenham meteorite is an olivine–hypersthene-rich (L6) chondrite (*11*) composed of olivine, orthoenstatite, diopside, plagioclase which has been partly converted into glass (maskelynite) in a solid-state transformation at high pressure, Fe-Ni alloy, and troilite. The meteorite has a network of shock-induced veins (where the veins are <1 mm thick), and these veins enclose rounded fragments of host minerals in a black matrix. We examined three shock veins with an analytical transmission electron microscope (ATEM). ATEM specimens were taken from the optical thin section, milled by Ar ions into thin foils, and coated with carbon.

Olivine grains in the walls of the veins and in fragments are partially or totally transformed to blue-colored ringwoodite (γ phase) (*12*) or wadsleyite (β phase) (*13*). The black matrix, which is considered to have been quenched from melt (*14*), is dominated by Al-bearing majorite and a lesser amount of magnesiowüstite. These phases indicate the generation of high pressures and high temperatures by shock compression related to an impact event.

Within two shock veins, we identified ilmenite adjacent to clinoenstatite in fragments. The ilmenite formed aggregates, with each grain <1.4 μm in length. With *d*-spacings, angles, and systematic extinctions of electron diffraction patterns from several grains, all possible indexings by high-pressure polymorphs of pyroxene [majorite, ilmenite, perovskite, clinoenstatite ($P2_1/c$), and orthoenstatite (*Pbca*)] were examined, and only ilmenite with space group ($R\bar{3}$) could explain all these diffraction patterns (Fig. 1). The estimated lattice parameters from several selected-area electron diffraction (SAED) patterns are $a = 0.478 \pm 0.005$ nm and $c = 1.36 \pm 0.01$ nm, assuming a hexagonal structure. These parameters agree with those extrapolated from the synthetic $(Mg,Fe)SiO_3$-ilmenite within the SAED accuracy (*15*). Also, the c/a ratio of 2.85 is nearly equal to that of synthetic ilmenite (c/a = 2.87). Chemical analyses of these grains were carried out with an energy-dispersive analytical system attached to the ATEM (Table 1), and we found that the ilmenite grains have similar compositions to the adjacent clinoenstatite grains.

Ilmenite grains in the Tenham meteorite have two morphologies. One is granular-shaped (<0.4 μm in length) (Fig. 2A), and the other is columnar (<1.4 μm in length) (Fig. 2B). Both types of grains do not show any microstructure except a low density of dislocations. Granular grains occur within the interstitial glassy phase. Assemblages of columnar grains have a brick-wall-like texture, and each grain is elongated along the same direction. Moreover, most of the columnar ilmenites have topotaxial relationships with adjacent clinoenstatite (Fig. 2C). The reciprocal c^* axis of ilmenite is parallel to the a^* axis of clinoenstatite. The ilmenite intergrown with clinoenstatite was observed in the other vein, and they also have the same topotaxial relationships. Clinoenstatite showed (100) twin lamellae, proba-

Table 1. Average chemical compositions of clinoenstatite, ilmenite, and perovskite. Compositions of ilmenite and perovskite were determined by ATEM and that of clinoenstatite by electron microprobe analysis. The number in parentheses for each phase is the number of analyses of the different grains.

Oxide (weight %)	Clinoenstatite (8)	Ilmenite* (6)	Perovskite* (3)
Na_2O	0.01	0.67	0.81
MgO	29.33	28.39	28.58
Al_2O_3	0.15	0.07	0.16
SiO_2	55.74	56.35	55.14
CaO	0.78	0.38	0.12
TiO_2	0.15	0.17	0.42
Cr_2O_3	0.16	0.16	0.18
MnO	0.51	0.28	0.19
FeO	13.51	13.54	14.41
Total	100.33	100	100
	Cation number (O = 6)		
Na	0.00	0.05	0.06
Mg	1.56	1.51	1.53
Al	0.01	0.00	0.01
Si	1.99	2.01	1.98
Ca	0.03	0.02	0.01
Ti	0.00	0.00	0.01
Cr	0.01	0.00	0.01
Mn	0.02	0.01	0.01
Fe	0.40	0.40	0.43
Total	4.01	4.01	4.03
Fe/(Mg + Fe)	0.21 ± 0.01	0.21 ± 0.01	0.22 ± 0.01

*Values were calculated by use of the experimentally determined K-values with synthetic corundum (Al_2O_3)–ilmenite ($MgSiO_3$) and silicate perovskite phases, respectively (*18*). K-values of some cation pairs for ilmenite were taken from the average K-values of pyroxene and silicate perovskite.

Division of Earth and Planetary Sciences, Graduate School of Science, Hokkaido University, Sapporo 060, Japan.

*To whom correspondence should be addressed. E-mail: tomioka@epms.hokudai.ac.jp

bly caused by transition from the original orthoenstatite (8).

Perovskite was also identified in the same occurrence as granular ilmenite (Fig. 3A). The SAED pattern of orthorhombic perovskite along the [010] zone axis (Fig. 3B) is consistent only with perovskite (*Pbnm*) in its *d*-spacings, angles, and systematic extinctions of the diffraction spots but could not be indexed by any other pyroxene polymorph. Estimated lattice parameters from the diffraction pattern are $a = 0.474 \pm 0.005$ nm and $c = 0.70 \pm 0.01$ nm, which is consistent with the values extrapolated from synthetic (Mg,Fe)SiO_3-perovskite determined by x-ray diffraction (*15*). The lattice parameter *b* could not be estimated, because we could observe only the a^*–c^* plane of the reciprocal lattice. The other indication that this phase is perovskite is its characteristic instability in the electron beam; the grains easily converted into an amorphous phase during electron-beam irradiation. The chemical composition is almost the same as those of adjacent clinoenstatite and ilmenite grains (Table 1). The existence of perovskite in the shock vein means the generated pressure was at least ~23 GPa (*16*). At such high pressures, orthoenstatite is not stable and is converted into clinoenstatite. If the generated temperature around the pyroxene grains was high enough, they would have further transformed into higher-pressure phases. This occurrence of the pyroxene-ilmenite or pyroxene-perovskite pair seems to reflect the heterogeneity of the generated temperature in fragments during the shock event.

We found majorite with 4.8 mole percent (mol%) of Al_2O_3 component [in the (Mg,Fe)SiO_3-Al_2O_3 join] distributed in the black matrix but not in contact with pyroxene in the fragments. The granular-shaped majorite grains were larger (up to 2 μm in length) than ilmenite or perovskite, and their interstices were filled with irregular-shaped magnesiowüstite. Magnesiowüstite is reported to occur also as inclusions in Al-bearing majorite in the Tenham chondrite (*14*). In contrast to this majorite, the ilmenite and perovskite do not have any Al. These differences in texture and Al content involved between majorite and ilmenite or perovskite may be caused by different reaction processes. The ilmenite and perovskite may have been transformed from almost Al-free pyroxene by a solid-state reaction during the shock event, whereas the majorite may have crystallized from the shock-induced melt, where most of the Al in the majorite may have been derived from molten plagioclase. We did not find any Al-free majorite as was previously reported for the Tenham meteorite (*8, 14*).

Ito and Yamada (*15*) reported that the solubility limit of $FeSiO_3$ in Al-free ilmenite and perovskite is nearly 10 mol% at 1100°C, and Fei *et al*. (*15*) concluded that the solubility limit of $FeSiO_3$ in perovskite is about 12 mol% at 26 GPa from 1150° to 1740°C. With the higher Fe content, Ito and Yamada (*15*) showed that single-phase ilmenite and perovskite are replaced by spinel + stishovite and perovskite + magnesiowüstite + stishovite, respectively. Compared with these solubility limits, the $FeSiO_3$ content of 20 to 22 mol% of ilmenite and perovskite phases present in the Tenham meteorite is significantly higher. Nevertheless, we observed no de-

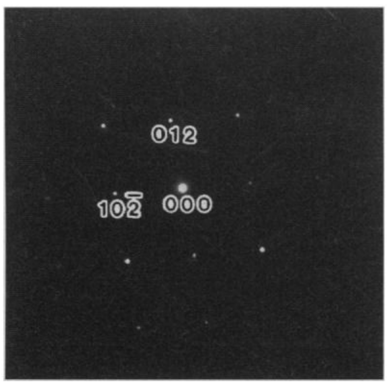

Fig. 1. SAED pattern of (Mg,Fe)SiO_3-ilmenite in a shock vein in the Tenham meteorite. Distances of 012 and 10$\bar{2}$ in the hexagonal setting from 000 on the film correspond to the *d*-spacings of 0.349 ± 0.005 nm and 0.351 ± 0.005 nm, respectively. This diffraction pattern can be indexed only by the ilmenite structure with space group ($R\,\bar{3}$).

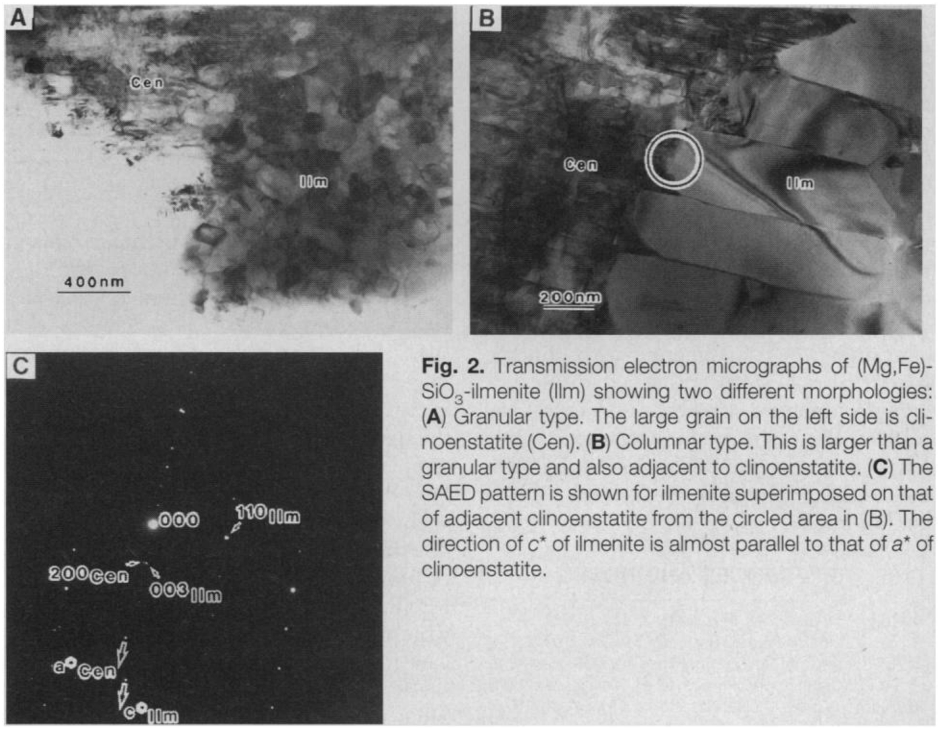

Fig. 2. Transmission electron micrographs of (Mg,Fe)-SiO_3-ilmenite (Ilm) showing two different morphologies: (**A**) Granular type. The large grain on the left side is clinoenstatite (Cen). (**B**) Columnar type. This is larger than a granular type and also adjacent to clinoenstatite. (**C**) The SAED pattern is shown for ilmenite superimposed on that of adjacent clinoenstatite from the circled area in (B). The direction of c^* of ilmenite is almost parallel to that of a^* of clinoenstatite.

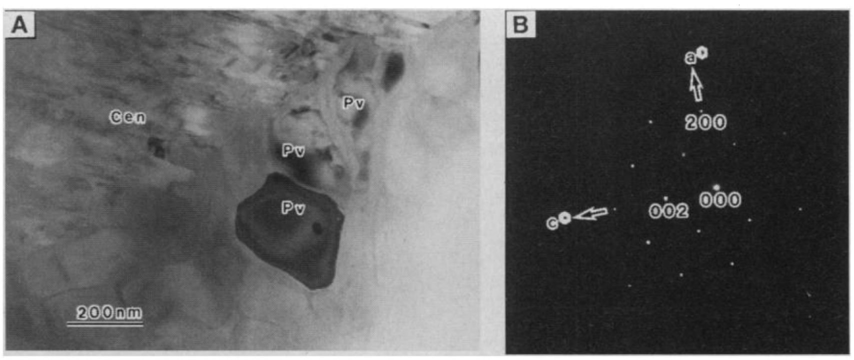

Fig. 3. Electron micrographs of (Mg,Fe)SiO_3-perovskite (Pv) adjacent to clinoenstatite. (**A**) Transmission electron micrograph. (**B**) The SAED pattern is shown along the [010] zone axis. Distances of 200 and 002 from 000 on the film correspond to the *d*-spacings of 0.236 ± 0.005 nm and 0.352 ± 0.005 nm, respectively.

composed phases around the ilmenite or perovskite grains. The peak pressure pulses may be on the order of 10^{-2} to 10^{-1} s in large-scale meteorite impacts (*17*), and the cooling rate will be very rapid. In such a short event, the decomposition of pyroxene into spinel + stishovite or perovskite + magnesiowüstite + stishovite would be difficult to complete in the solid state. Therefore, pyroxene probably transformed metastably into high-Fe ilmenite and perovskite without producing these other phases.

The shock event must also have affected the transformation mechanism. For the topotaxial relationship of $(100)_{Cen}$ // $(0001)_{Ilm}$, where subscripts Cen and Ilm denote clinoenstatite and ilmenite, respectively, both planes correspond to the close-packed layers of oxygen for their respective phases (approximate cubic close-packed for clinoenstatite and hexagonal close-packed for ilmenite). Therefore, in the transition from clinoenstatite to ilmenite, the close-packed layers of oxygen are preserved, characteristic of shear transformation. Probably, the rapid transformation by the shock event favored the shear transformation mechanism for the clinoenstatite-ilmenite transition. This topotaxial relation indicates that this process may have proceeded by the displacement of the close-packed layers of oxygen on (100) plane for clinopyroxene. The intergrowth of ilmenite with clinopyroxene also suggests this mechanism. The granular ilmenite, which has no topotaxial relationship with clinoenstatite, would have formed by the nucleation and growth mechanism, probably under the slower cooling rates.

REFERENCES AND NOTES

1. L. G. Liu, *Geophys. Res. Lett.* **2**, 417 (1975).
2. ______, *Earth Planet. Sci. Lett.* **31**, 200 (1976).
3. E. Ito and Y. Matsui, in *High-Pressure Research: Applications in Geophysics*, M. H. Manghnani and S. Akimoto, Eds. (Academic Press, New York, 1977), pp. 193–208.
4. T. Kato and M. Kumazawa, *Nature* **316**, 803 (1985).
5. H. Sawamoto, in *High-Pressure Research in Mineral Physics*, M. H. Manghnani and Y. Syono, Eds. (Terra Scientific Publishing/American Geophysical Union, Tokyo/Washington, DC, 1987), pp. 209–219.
6. B. Mason, J. Nelen, J. S. White Jr., *Science* **160**, 66 (1968).
7. L. C. Coleman, *Can. Miner.* **15**, 97 (1977).
8. G. D. Price, A. Putnis, S. O. Agrell, *Contrib. Mineral. Petrol.* **71**, 211 (1979).
9. ______, D. G. W. Smith, *Can. Mineral.* **21**, 29 (1983).
10. M. Chen, T. G. Sharp, A. El Goresy, B. Wopenka, X. Xie, *Science* **271**, 1570 (1996).
11. L6 is the most metamorphosed chondrite as judged by the Van Schmus and Wood classification. See W. R. Van Schmus and J. A. Wood, *Geochim. Cosmochim. Acta* **31**, 747 (1967).
12. R. A. Binns, R. J. Davis, S. J. B. Reed, *Nature* **221**, 943 (1969).
13. A. Putnis and G. D. Price, *ibid.* **280**, 217 (1979).
14. H. Mori and H. Takeda, *Lunar Planet. Sci.* **XVI**, 579 (1985).
15. Extrapolated lattice parameters of $(Mg_{1-x},Fe_x)SiO_3$-ilmenite and -perovskite with $x = 0.2$ from those of the synthetic samples are $a = 0.473$ and $c = 1.359$ nm ($c/a = 2.873$) and $a = 0.480$ and $c = 0.691$ nm, respectively. Data of synthetic samples were taken from E. Ito and H. Yamada [in *High-Pressure Research in Geophysics*, S. Akimoto and M. H. Manghnani, Eds. (Center for Academic Publications, Tokyo, 1982), pp. 405–419] and Y. Fei, Y. Wang, and L. W. Finger [*J. Geophys. Res.* **101**, 11525 (1996)]. Taking the accuracy of the lattice parameters from the SAED pattern into account, they agree well with the extrapolated values, and still rule out the possibilities of any other polymorph of $(Mg,Fe)SiO_3$.
16. See E. Ito and E. Takahashi, *J. Geophys. Res.* **94**, 10637 (1989). They showed that $MgSiO_3$-perovskite is stable at pressures ≥23 GPa at 1600°C. Its stability limit can be affected by temperature and Fe content. Therefore, we estimated the lower limit of pressure as 23 GPa.
17. D. Stöffler, *Fortschr. Mineral.* **49**, 50 (1972).
18. K. Fujino, N. Miyajima, T. Yagi, T. Kondo, N. Funamori, in *Proceedings of the U.S.–Japan Seminar*, Maui, HI, 22 to 26 January 1996, M. H. Manghnani and T. Yagi, Eds. (American Geophysical Union, Washington, DC, in press).

19. We thank Y. Syono and N. Miyajima for helpful comments and T. Kuwajima and R. Tanaka for technical assistance. Supported by a Grant-in-Aid for Research (no. 06402019) from the Ministry of Education, Science, and Culture of the Japanese Government.

15 April 1997; accepted 11 July 1997

Size Variation in Middle Pleistocene Humans

J. L. Arsuaga,* J. M. Carretero, C. Lorenzo, A. Gracia, I. Martínez, J. M. Bermúdez de Castro, E. Carbonell

It has been suggested that European Middle Pleistocene humans, Neandertals, and prehistoric modern humans had a greater sexual dimorphism than modern humans. Analysis of body size variation and cranial capacity variation in the large sample from the Sima de los Huesos site in Spain showed instead that the sexual dimorphism is comparable in Middle Pleistocene and modern populations.

Sexual dimorphism is potentially a major source of size variation in a population (*1*, *2*). Most samples in the human paleontological record consist of specimens that span large chronologic and geographic ranges; consequently, interpopulational variation, directional trends, or diachronic fluctuations can contribute more to the sample variation (even if the sample is large) than sexual dimorphism.

In the Sima de los Huesos site in Sierra de Atapuerca, Spain, there is a large sample of human fossils that comes from a single Middle Pleistocene biological population, which provides an opportunity to investigate intrapopulational variation (*3*, *4*). All skeletal elements are represented in the Sima de los Huesos human collection in large numbers, and the minimum number of individuals has been estimated at 32 on the basis of the dental sample (*5*). The fossils have been directly dated by U-series and electron spin resonance to more than 200,000 years ago, and the probable age is >300,000 years ago (*6*). These dates are compatible with the faunal content of the site (*7*). The Sima de los Huesos hominids are attributed to *Homo heidelbergensis* and correspond to a population ancestral to Neandertals, exhibiting a mosaic of primitive traits, combined with some (in general, incipient) Neandertal-derived traits (*3*, *4*).

Although many methods have been designed to evaluate the degree of sexual dimorphism (*2*), their calculations are based on individuals of known sex or skeletally diagnosed sex. A problem in paleoanthropology is that sexual dimorphism is determined on the same feature (size) used for sex diagnosis and presupposes sexual dimorphism in order to estimate itself. Some researchers have concentrated instead on a statistical approach in which the likelihood of obtaining by chance a fossil sample with a given variation is calculated (*8*). It is in essence a hypothesis test in which the null hypothesis is the variation of a living species analog. If none or few samples randomly generated from the extant species show a variation greater than that of the fossil sample, the null hypothesis (that is, the hypothesis that the variation of the fossil species is the same or less than that of the extant species) is rejected. Following this statistical approach we used the bootstrap method (*9*) to compare the intrapopulation variation between the Sima de los Huesos

J. L. Arsuaga, C. Lorenzo, A. Gracia, I. Martínez, Departamento de Paleontología, Instituto de Geología Económica, Facultad de Ciencias Geológicas, Universidad Complutense de Madrid, Ciudad Universitaria 28040 Madrid, Spain.
J. M. Carretero, Departamento de Ciencias Históricas y Geografía, Facultad de Humanidades y Educación, Universidad de Burgos, 09071 Burgos, Spain, and Laboratory for Human Evolutionary Studies, Museum of Vertebrate Zoology, 3101 Valley Life Sciences Building, Berkeley, CA 94720–3160, USA.
J. M. Bermúdez de Castro, Museo Nacional de Ciencias Naturales, Consejo Superior de Investigaciones Científicas, José Gutiérrez Abascal 2, 28006 Madrid, Spain.
E. Carbonell, Laboratori d'Arqueologia, Universitat Rovira i Virgili, Plaza Imperial Tarraco 1, 43005 Tarragona, Spain.

*To whom correspondence should be addressed.